Nanoscale

Valence and Oxide Impurities in MoS2 and WS2 Dramatically Change Its Electrocatalytic Activity Towards Proton Reduction

Journal:	*Nanoscale*
Manuscript ID	NR-ART-04-2016-003086.R1
Article Type:	Paper
Date Submitted by the Author:	29-Jul-2016

Complete List of Authors:	BINTE MOHAMAD LATIFF, Naziah; Nanyang Technological University, Chemistry and Biological Chemistry Wang, Lu; Nanyang Technological University, Chemistry and Biological Chemistry Mayorga-Martinez, Carmen; Nanyang Technological University, Chemistry and Biological Chemistry Sofer, Zdenek; Institute of Chemical Technology, Prague, Department of Inorganic Chemistry Fisher, Adrian; University of Cambridge, Chemical Engineering and Biotechnology Pumera, Martin; Nanyang Technological University, Chemistry and Biological Chemistry

Journal Name

ARTICLE

Valence and Oxide Impurities in MoS_2 and WS_2 Dramatically Change Its Electrocatalytic Activity Towards Proton Reduction

Received 00th January 20xx,
Accepted 00th January 20xx

DOI: 10.1039/x0xx00000x

www.rsc.org/

Naziah Mohamad Latiff,[a] Lu Wang,[a] Carmen C. Mayorga-Martinez,[a] Zdeněk Sofer,[b] Adrian C. Fisher,[c] Martin Pumera[a]

Layered molybdenum disulfide (MoS_2) and tungsten disulfide (WS_2) received renewed interest in recent years as they are catalytic towards hydrogen evolution reaction (HER) and they are touted as future replacements of platinum in electrolyzers. There is significant discrepancy in the found onset potentials of MoS_2 and WS_2 towards hydrogen evolution reaction. Here we show that presence of valence sulfide impurities, such as MoS_3 and WS_3, and their oxide counterparts, such as MoO_2, MoO_3 and WO_2, WO_3 can contribute to the catalytic activity towards hydronium reduction to hydrogen of MoS_2 and WS_2. Therefore, it is highly possible that the differences in the reported onset potentials and thus catalytic activities of the MoS_2 and WS_2 are due to presence of catalytic impurities.

Introduction

With global warming, climate change and depleting supply of limited fossil fuels, there is an urgent need for us to develop on clean (low CO_2 emissions), sustainable and renewable sources of energy. However, the intermittent and uncontrolled nature of renewable sources of energy prompts energy storage systems to play a greater role in our lives. One attractive solution is the conversion of excess electrons to hydrogen gas, a high energy density carrier gas, in a process known as hydrogen evolution reaction (HER). However, this method typically requires expensive and scarce platinum-based electrocatalysts to drive the reaction efficiently, thereby imposing economic constraints for its wide spread practical implementation. As such, there is intensive research for alternative materials to replace platinum as HER electrocatalysts.[1-3]

In this quest, layered molybdenum disulfide (MoS_2), tungsten disulfide (WS_2) and their related materials have demonstrated promising HER activities close to Pt.[2,4-8] Through a variety of synthetic routes and strategies, a wide range of performances for MoS_2 and WS_2 has been reported in terms of overpotential at -10 mA/cm^2 current density and Tafel slope results.[2,8] Recently, there were reports that amorphous molybdenum sulfides (MoS_x), with compositions typically closer to MoS_3 compared to MoS_2, display excellent HER activities.[9-13] The same is true about WS_2 and corresponding WS_x compounds.[14] MoS_3 and corresponding Mo(IV) and Mo(VI) oxides are typical impurities in MoS_2 materials; similar to the case of WS_2.[2,14-18] Such findings triggered us to explore the possible effects of MoS_3, MoO_2/MoO_3 impurities (and their tungsten counterparts), which may be formed during synthesis or storage, in affecting HER performances of MoS_2 and WS_2 materials.[17] Here, we investigate the effects of different possible valence and oxide impurities in MoS_2 and WS_2 on their HER catalysis, in terms of affecting their overpotentials, Tafel slope values as well as the shape of the polarization curves. Following that, we identify the Mo- and W-based impurities which show highly catalytic effect towards hydrogen evolution reaction and therefore may be responsible for the large disparity of reported potentials of catalytic hydrogen evolution on MoS_2 (and WS_2) surfaces.

To achieve this aim, we first characterized MoS_2, WS_2 and their possible synthetic impurities using scanning electron microscopy (SEM), energy-dispersive spectroscopy (EDS) and X-ray photoelectron spectroscopy (XPS). We have identified the possible synthetic impurities of MoS_2 and WS_2 to be their oxidized moieties (i.e. MoS_3, MoO_2, MoO_3, WS_3, WO_2, WO_3) due to the use of oxides as starting precursors, or possible oxidation during reaction conditions or prolonged exposure.[18-22] After material characterization, their HER performances were compared. Subsequently, we prepared physical mixtures of various impurities with MoS_2 and WS_2 to study the effect of different impurities on the overpotential, Tafel slope and shape of HER polarization curves.

[a] N. M. L.; L. W.; C. M. M. and Prof. Dr. M. Pumera
Division of Chemistry and Biological Chemistry,
School of Physical and Mathematical Sciences,
Nanyang Technological University, Singapore
E-mail: pumera.research@gmail.com
[b] Prof. Z. Sofer
Department of Inorganic Chemistry,
University of Chemistry and Technology, Prague
[c] Prof. A. C. Fisher
Department of Chemical Engineering and Biotechnology,
University of Cambridge, UK

Electronic Supplementary Information (ESI) available: [details of any supplementary information available should be included here]. See DOI: 10.1039/x0xx00000x

Results and discussion

To verify the materials used for study, we first conducted material characterization using several techniques. SEM images of MoS_2, WS_2 and their possible synthetic impurities are shown in Fig. 1 and Fig. 2. Their SEM images display the typical layered structures as expected. The remaining materials (i.e. MoS_3, MoO_2, MoO_3, WS_3, WO_2, WO_3) show amorphous structures, with MoS_3, WS_3 and WO_3 displaying distinctly non-crystalline structures amongst them.

We used MoS_2 and WS_2 in their bulk forms in order to minimize the variation in properties seen upon exfoliation.[23-24] For example, in the case of bulk MoS_2 exfoliation *via* Li intercalation, a phase change from semiconducting to metallic MoS_2 has been reported.[25] This would also allow a better comparison between the different materials as their valence and oxide forms were not exposed to exfoliation conditions.

EDS analysis (S1-S2) is further used to verify the composition of the materials. In addition, XPS (Fig. 3) was performed to probe into their detailed bonding information. For Mo 3d deconvolution[26], Mo^{4+} and Mo^{6+} doublet peaks were observed to be around 229.5 eV, 232.6 eV and 232.3 eV, 235.4 eV respectively whereas for W 4f deconvolution[26], W^{4+} and W^{6+} doublet peaks were found at approximately 32.9 eV, 35.0 eV and 35.8 eV, 37.9 eV respectively. The deconvolution analysis for the high resolution S 2p spectra[27-28] shows the presence of S^{2-} terminal doublet peaks to be at 162.3 eV, 163.4 eV to be dominant in compounds with metal 6+ oxidation state (i.e. MoS_3, WS_3) while those with metal 4+ oxidation state (i.e. MoS_2 and WS_2) have prevalent S^{2-} bridging double peaks at 163.0 eV, 164.2 eV. The XPS characterization shows that whilst MoS_2 is pure, WS_2 contains slight W(VI) impurities.

The as-prepared MoS_2, WS_2 and their mixtures were also characterized to probe into the morphology and composition of prepared samples. SEM images of the as-prepared mixtures reveal presence of amorphous structures of MoS_3 and WS_3 dispersed randomly over surfaces of bulk layered MoS_2 and WS_2 sheets (S3), while their EDS mapping confirms the presence of transition metal and chalcogen elements in the prepared samples (S4-S5).

After material characterization, the hydrogen evolution activity of the materials was evaluated using linear sweep voltammetry (LSV) in 0.5 M H_2SO_4 (aq). Fig. 4 presents the result obtained from the electrochemical analysis. From this figure, MoS_3 and WS_3 show better catalytic performances compared to metal oxides, with 370 mV and 704 mV overpotentials achieved at -10 mA/cm^2 current density respectively. It appears that compounds with higher metal oxidation state (6+) and higher S content (i.e. MoS_3 and WS_3) offers better HER catalytic performance compared to those of lower metal oxidation state and lower S content. This observation is in line with other previous reports which found that MoS_3 and WS_3 give better HER activities compared to MoS_2 and WS_2.[11,17] With reference to the XPS results gathered, comparison between XS_3 and XS_2 compounds (where X

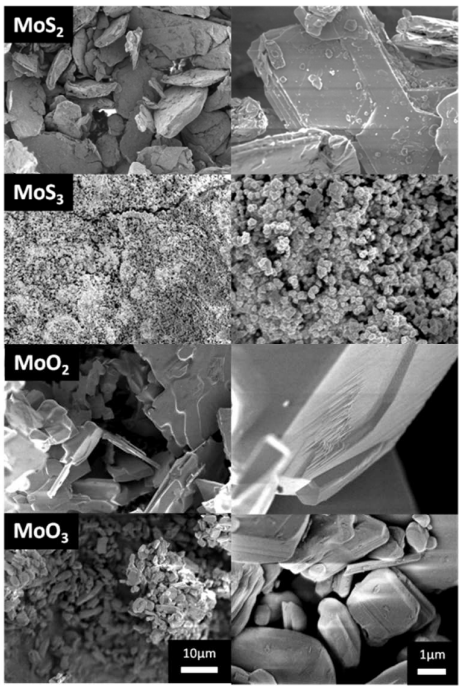

Fig. 1 SEM images of MoS_2 and their possible impurities during synthesis (MoS_3, MoO_2, MoO_3) at 2000× (left) and 15000× (right) magnifications. Scale bars representing 10 μm and 1 μm are shown at the bottom images.

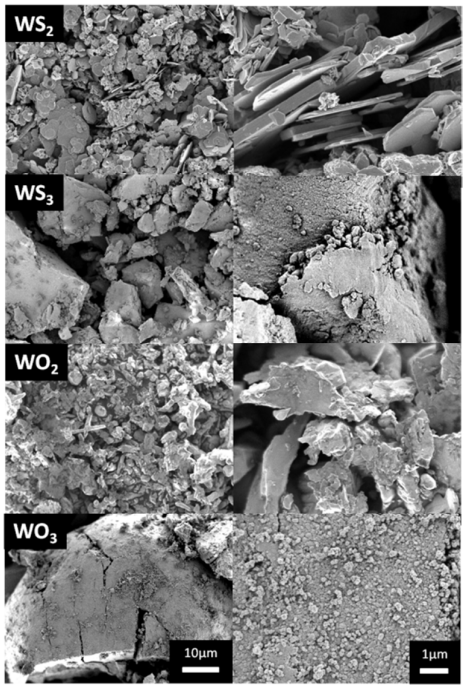

Fig. 2 SEM images of WS_2 and their possible impurities during synthesis (WS_3, WO_2, WO_3) at 2000× (left) and 15000× (right) magnifications. Scale bars representing 10 μm and 1 μm are shown at the bottom images.

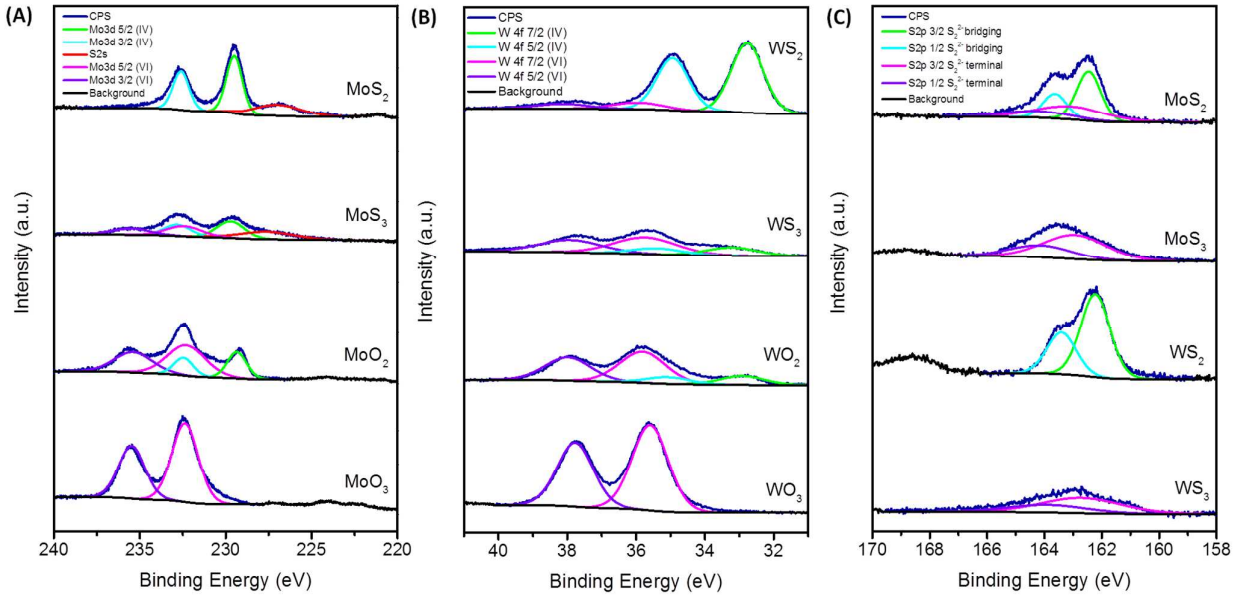

Fig. 3 X-ray photoelectron spectroscopy (XPS) spectra for the materials under study: (A) High-resolution Mo 3d spectra for Mo compounds (MoS_2, MoS_3, MoO_2 and MoO_3), (B) high-resolution W 4f spectra for W compounds (WS_2, WS_3, WO_2 and WO_3), and (C) high-resolution S 2p spectra for S-containing compounds (MoS_2, MoS_3, WS_2 and WS_3).

represents the metal Mo or W) suggests that higher HER performances could be linked to the presence of S^{2-} terminal bonds (see high resolution XPS S 2p spectra in Fig. 3).

In order to elucidate the HER mechanisms for the various materials tested, we calculated the Tafel slope values from their corresponding HER polarization curves. Tafel slope values can allow us to discern the mechanism and rate-determining step (RDS) for the reaction as different range of values would indicate different RDS steps. For bulk MoS_2 and WS_2, their Tafel slope values were determined to be 179 and 174 mV/dec respectively, similar to those reported in literatures.[23-24] These results show that in their bulk states, the HER process for MoS_2 and WS_2 is limited by the Volmer step (electrochemical adsoprtion step). In contrast, MoS_3 and WS_3 have lower Tafel slope values of 75 mV/dec and 109 mV/dec respectively, suggesting a different HER mechanism involved. The lower Tafel slopes achieved by the metal trisulfides could be attributed to their lower crystallinity as reported by a study by Li et. al.[29] This is also observed in this work by WO_3 that yields a remarkably low Tafel slope value of 38 mV/dec which also shows an amorphous structure. This Tafel slope value is interesting as it is close to that reported for the best well known performing HER electrocatalyst (Pt); 30 mV/dec[30]. This could be the reason for its increasing exploration for HER applications[31-35] However, its overpotential at -10 mA/cm^2 current density is relatively high at 561 mV in comparison with Pt which has almost zero overpotential.[8]

After identifying MoS_3 and WS_3 to be catalytically active towards HER, we proceeded to systematically study the potential effect of heterogeneous valence impurities. We created physical mixtures of MoS_2 and WS_2 with a wide variety of metal (VI) sulfide impurities (i.e. 1, 2.5, 5, 7.5, 10, 12.5, 15, 20, 25, 50, and 75%) to investigate their electrocatalytic effect on hydrogen evolution. The data gathered in Fig. 5 show that increasing amounts of MoS_3 and WS_3 impurities can decrease the overpotential at -10 mA/cm^2 current density. In other words, different amounts of MoS_3 and WS_3 can cause variation in the HER performance of MoS_2 and WS_2 materials in the positive direction, that is towards lower overpotentials. This provides an explanation for the wide range of overpotentials reported for molybdenum and tungsten disulfides across different synthesis methods. From the wide range of concentrations tested, we are able to identify 12.5% MoS_3 and 25% WS_3 as the optimal proportions of impurities in the transition metal disulfides, where the effect of additional impurities in lowering the overpotential of the overall catalyst becomes less significant beyond these concentrations (Fig. 5B).

In terms of Tafel slope, we observe an interesting decrease in value with a mere 1% of MoS_3 introduced (Fig. 5D). With further increase in the metal trisulfide content, however, the Tafel slope values remain relatively constant. This can also be seen for its tungsten counterpart. This suggests that composition does not influence Tafel slope values as much as a low degree of crystallinity, in agreement with another study.[29] Most importantly, our findings show that small traces of amorphous MoS_3/WS_3 is sufficient to significantly alter the HER mechanism of MoS_2 and WS_2.

Besides studying the effects of MoS_3 and WS_3 impurities on overpotential and Tafel slope values, the effect of these

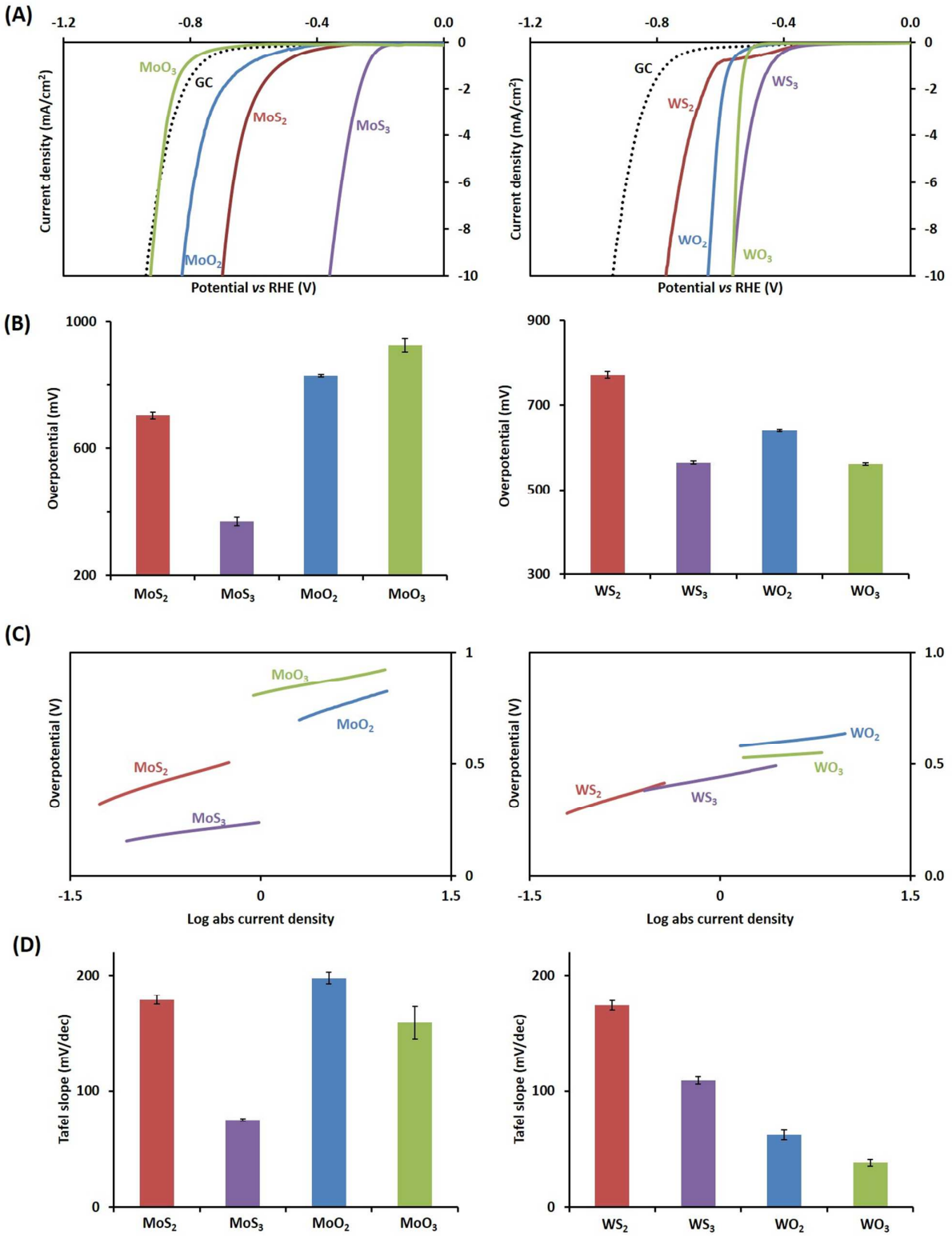

Fig. 4 Hydrogen evolution for MoS_2, WS_2 and their possible impurities during synthesis (MoS_3, MoO_2, MoO_3, WS_3, WO_2, WO_3) tested in 0.5 M H_2SO_4 at a scan rate of 2 mV/s: (A) HER polarization curves of the various compounds tested, (B) bar charts comparing their overpotentials at -10 mA/cm^2 current density, (C) their corresponding Tafel plots, and (D) bar charts comparing their calculated Tafel slope values.

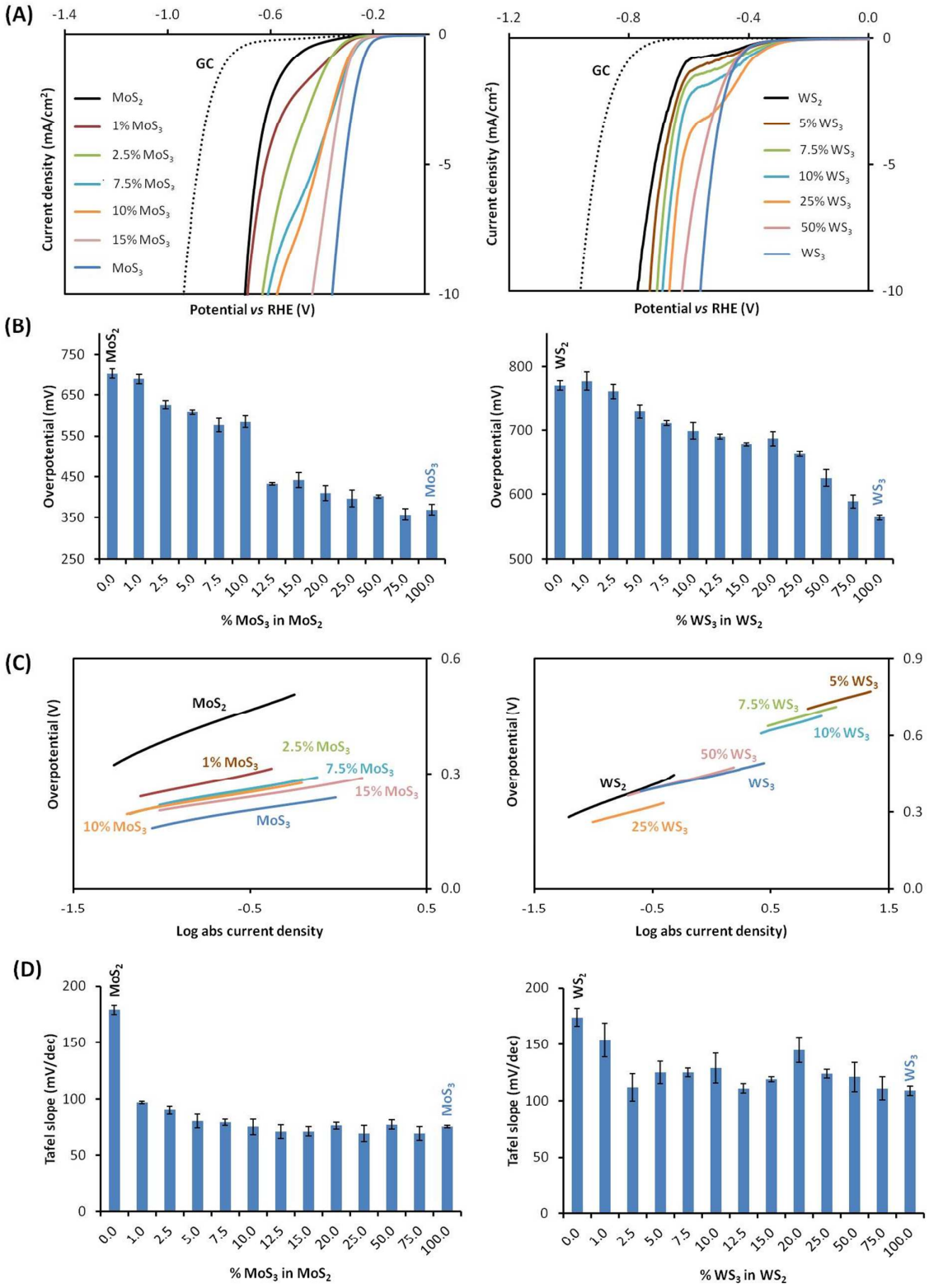

Fig. 5 Linear scan voltammetery (LSV) measurements for MoS_2 with different amounts of MoS_3 impurities (left), and WS_2 with different amounts of WS_3 impurities (right): (A) HER polarization curves of the various compounds tested, (B) bar charts comparing their overpotentials at -10 mA/cm^2 current density, (C) their corresponding Tafel plots, and (D) bar charts comparing their calculated Tafel slope values. For better clarity, only five concentrations of mixtures are presented for comparison of LSVs in graph (A).

impurities on the shape of HER polarization curves was also explored. Fig. 5 shows that small amounts of MoS_3 in MoS_2 can give rise to pre-waves in their LSV curves. Interestingly for WS_2, the unmixed sample itself showed a slight dip in LSV which significantly lowers the onset potential (defined as overpotential recorded at -0.1 mA/cm^2) to be close to that measured for WS_3 (WS_2 onset: 322 mV, WS_3 onset: 305mV). This early dip in LSV could be attributed to the slight W(VI) impurities as detected in WS_2 by XPS analysis (Fig. 3). Similarly, mixtures of WS_3 in WS_2 also showed pre-waves in their LSVs. This observation provides evidence that physical mixtures of catalytic impurities can alter the shape of HER polarization curves. In addition, different amounts of catalytic impurities are required to produce alteration in the shape of LSVs for MoS_2 and WS_2 materials. For MoS_2, the pre-waves are observed with the presence of 1 to 10% MoS_3 whereas for its W counterpart, the concentration range was found to be between 0 to 25% WS_3.

Pre-waves observed in LSVs in published works had previously been attributed to the inherent electrochemistry or different catalytic sites of a material[23] as well as a reduction of structural defects such as oxidized metal clusters[36]. In this study, we provide evidence that these pre-waves may arise due to the presence of valence impurities. Apart from valence impurities, we had also tested mixtures with the oxide impurities. For WO_2 and WO_3, which have intermediate HER activities between that of WS_3 and bulk WS_2, slight pre-waves were observed from their LSVs (S6). However, for MoO_2 and MoO_3 which were found to be less catalytic than its metal disulfide, no pre-waves in the LSVs were seen (S7). This suggests that pre-waves in the LSVs could be due to the presence of more catalytic impurities instead of less active ones.

In order to understand the origin behind the better HER performances seen for MoS_3 and WS_3, as well as their mixtures with the metal disulfides, we performed electrochemical impedance spectroscopy (EIS) to compare their charge transfer resistances (R_{CT}). Nyquist plots (Fig. 6) revealed that the metal trisulfides show marked improvements in conductivities as seen from their significantly lower R_{CT} values (MoS_3: 0.2 kΩ, WS_3: 0.2 kΩ) as compared to the metal disulfides (MoS_2: 48.8 kΩ, WS_2: 8.4 kΩ). Since the electrocatalytic reaction involves charge transfer processes between electrons from the glassy carbon surface to the surface of the catalyst, and subsequently from the catalyst surface to protons in the electrolyte solution, an enhancement in electron conductivity would greatly improve the HER catalysis. Similarly, small amounts of MoS_3/WS_3 present in their metal disulfides results in low R_{CT} values (10% MoS_3: 1.1 kΩ, 10% WS_3: 1.3 kΩ). This suggests that the presence of small traces of such metal trisulfides (MoS_3/WS_3) can noticeably lower charge transfer resistance of molybdenum and tungsten disulfides, thereby dominating their electrochemistry. This noticeable lowering R_{CT} thus means facile electron transfer for proton reduction at MoS_2/MoS_3 and WS_2/WS_3 mixtures and influences rate determining step of the reaction. Consequently, this is translated to a decrease in Tafel slope values as observed in Fig. 5D. The Tafel slope values seen in Fig. 5D could also be explained by these EIS data. With similar R_{CT} values between

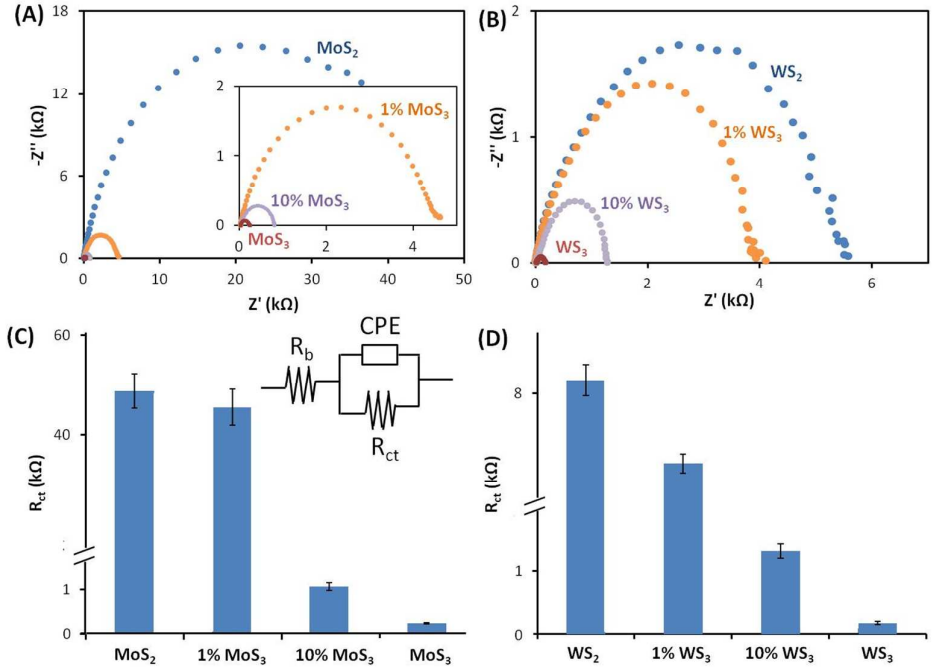

Fig. 6 Electrochemical impedance spectroscopy (EIS) measurements conducted for (A) MoS_2, 1% MoS_3 in MoS_2, MoS_3 as well as their (B) W counterparts. Bar charts (C) and (D) compares the resistances (R_{ct} values) for the various samples tested. R_{ct} represents charge transfer resistance, R_b is short for bulk resistance while CPE

stands for constant phase element. The Nyquist plots were measured at frequencies between 10000 kHz to 0.1 Hz and at an overpotential of 500 mV for MoS_2/MoS_3 and 750 mV for WS_2/WS_3.

mixtures containing small traces of metal trisulfides and the pure metal trisulfides, they are all likely to have similar RDS and therefore similar Tafel slope values as observed.

For the charge transfer between catalyst surface and protons in the electrolyte solution, it is facilitated by catalyst active sites. For layered transition metal dichalcogenides (TMDs) MoS_2 and WS_2, it has been well reported that the unsaturated S and/or metal (Mo, W) edge sites are the catalytic sites for their HER activity, while the basal planes are inert.[17] On the contrary, for amorphous transition trisulfides, their structures and HER active sites have not been well understood yet. Previously, several groups have suggested that the active sites for amorphous molybdenum sulfides (MoS_x, MoS_3) to be similar to that for amorphous molybdenum sulfide clusters; that is the S edge sites (in this case the bridging S_2^{2-} and terminal S^{2-}).[29] In a more recent study, Tran et. al. reported amorphous molybdenum sulfides as molecular-based coordination polymers build up from discrete $[Mo_3S_{13}]^{2-}$ units that are linked together by two terminal disulfide (S_2^{2-}) ligands with a third free terminal disulfide ligand available to generate HER active molybdenum hydride moieties.[36] Meanwhile, its tungsten counterpart is even less studied but similar inferences have been made due to their resemblances.[17] In any case, the amorphous nature of the metal trisulfides is likely to expose more of these catalytic edge sites, to facilitate for better HER activities.[17] From the numerous successful catalyst design strategies seen in literature, it has been well established that exposing more active sites for reaction is an effective concept to improve the HER performance of MoS_2 and WS_2 materials. This includes disorder engineering[37-38], vertically aligned TMDs[39-40], and synthesis of nanoflowers[41], nanoflakes[42], nanoparticles[5,43] as well as mesoporous structures[44]. Therefore, it is reasonable to deduce that the amorphous structures of MoS_3 and WS_3 which give rise to larger specific areas of the metal trisulfides can expose more catalytically edge sites thereby resulting in enhanced HER activities. These evidences highlight the importance of structure and conductivity in the design of HER electrocatalysts.

Previously, Xie et. al. had successfully modulated these two factors in molybdenum disulfide nanosheets through varying different synthesis temperatures.[37] The authors achieved an optimum balance between degree of structural defects and conductivity through incorporation of conductive $Mo^{(IV)}$-O species at different synthesis temperatures. In comparison with their work, our results may seem contradictory as we found that physical mixtures of MoO_2 in bulk MoS_2 did not improve the HER performance of the molybdenum disulfide (Figure S7). However, this could be due to different effects arising from the bulk nature of TMDs in our study. Nevertheless, both our findings agree that structural and electronic effects play important roles for efficient HER electrocatalysts. While this was achieved through finding a balance between degree of structural defects and incorporation of conductive $Mo^{(IV)}$-O species in their work, here we showed that physical mixtures of amorphous and conductive MoS_3 can also enhance the HER activity of the molybdenum disulfides.

Conclusions

In summary, we have demonstrated that even small amounts of catalytic impurities of Mo or W trisulfides can cause pre-waves in the voltammogram and that only 10% of such trisulfides can completely dominate the electrochemistry of corresponding transition metal dichalcogenides. These findings highlight the effects of impurities during material synthesis of MoS_2 and WS_2 materials for hydrogen evolution application and aid our understanding to the observed HER behaviour of the material. In addition, these findings can serve as a platform for us to further develop on the catalytic activities of these materials.

Experimental section

Materials

Bulk molybdenum (IV) sulfide powder (<2 µm, 99 %), molybdenum (IV) oxide powder (99 %), molybdenum (VI) oxide powder (99.97 %), tungsten (IV) oxide powder (-100 mesh, 99.99 %), and tungsten (VI) oxide powder (99.9 %) were purchased from Sigma-Aldrich, Singapore while bulk tungsten (IV) sulfide (99.8 %) and molybdenum (VI) sulfide dehydrate were obtained from Alfa Aesar (Germany). Ammonium heptamolybdate tetrahydrate (99.5%), sodium tungstate dihydrate (99.5%), hydrochloric acid (35%), acetone (99.9%) and carbon disulfide (99.99%) was obtained from Penta, Czech Republic. Selenium (99.5%) and aluminium (99.7%) were obtained from STREM, Germany. H_2S (99.5%) and argon (99.999%) were obtained from SIAD, Czech Republic.

Synthesis of WS_3

Synthesis was performed by acidic decomposition of ammonium tetrathiotungstate. 25 g of sodium tungstate dihydrate was dissolved in 250 mL of water. Subsequently, 100 mL of 1 M hydrochloric acid was slowly added to the solution. Tungstic acid that was formed was purified by repeated decantation and centrifugation. Thereafter, tungstic acid was separated by suction filtration, washed with water and dried in a vacuum oven at 50 °C for 48 hours. Following that, 10 g of tungstic acid was dissolved in 100 mL of concentrated ammonia and filtered using 450 nm nylon membrane. The solution was then bubbled with H_2S gas for 10 hours (about 200 mL/min). After which, red crystals of ammonium tetrathiotungstate formed were separated by suction filtration and washed with cold water. To 5 g of $(NH_4)_2WS_4$ in 5 wt.% of ammonia solution, 1 M solution of hydrochloric acid was

slowly added to the mixture with vigorous stirring and under argon atmosphere. WS_3 formed was then separated by suction filtration and washed with water followed by acetone. WS_3 was subsequently dried under vacuum at 50 °C for 24 hours. Later, WS_3 was dispersed in carbon disulfide and repeatedly decanted to remove excess of sulphur. Finally, WS_3 was separated by suction filtration, washed with carbon disulfide and dried in vacuum oven at 50 °C for 48 hours.

Material characterization

Scanning electron microscopy (SEM) was performed using a field-emission scanning electron microscope (JOEL, Japan) in gentle-beam high mode at 2 kV (for MoS_2, MoO_2, WS_2) and 1 kV (for the remaining materials: MoS_3, MoO_3, WS_3, WO_2, WO_3). For the SEM of the as-prepared samples, SEM mode was used at 2 kV. Energy dispersive X-ray spectroscopy (EDS) data were obtained at an accelerating voltage of 15 kV. X-ray photoelectron spectroscopy (XPS) analyses were performed using a Phoibos 100 spectrometer and a monochromatic Mg X-ray radiation source (SPECS, Germany). Samples were prepared by coating carbon tapes with a uniform layer of the graphene materials under study.

Electrochemical measurement

All electrochemical hydrogen evolution reaction (HER) measurements were performed using Linear Sweep Voltammetry (LSV) with an Autolab PGSTAT101 electrochemical analyzer (Eco Chemie, The Netherlands). A three-electrode configuration electrode system at room temperature was used to measure the HER activity of the materials in aq. H_2SO_4 (0.5M) using a 5 mL electrochemical cell at a scan rate of 2 mV/s. A glassy carbon (GC) electrode was used as the working electrode, a platinum electrode served as the auxiliary electrode and an Ag/AgCl served as the reference electrode. All electrochemical potentials herein were reported versus the Ag/AgCl reference electrode. Prior to immobilization of the graphene samples onto the working electrode, suspensions of the materials were prepared in N,N–dimethylformamide to achieve a 5 mg mL^{-1} concentration, followed by a 20 min sonication. For mixtures, the prepared suspensions of various materials were physically mixed and sonicated for another 20 min to obtain a homogenous solution. Subsequently, 1 µL aliquot of the appropriate suspension (5 µg) was deposited onto the GC electrode surface. Upon evaporation of the solvent at room temperature, the LSV measurement was conducted. The GC electrode surfaces were renewed by polishing with alumina particles (0.05 mm) on a polishing pad and washed with distilled water of 18.2 MΩ cm resistivity. The Nyquist plots were measured at frequencies between 10000 kHz to 0.1 Hz and at an overpotential of 500 mV for MoS_2/MoS_3 and 750 mV for WS_2/WS_3. The impedance data was fitted to a simplified Randles circuit to obtain the series and charge-transfer resistances.

Acknowledgements

This research was supported by the National Research Foundation, Prime Minister's Office, Singapore under its Campus for Research Excellence and Technological Enterprise (CREATE) programme for funding.

Notes and references

1 X. Zou, Y. Zhang, *Chem. Soc. Rev.*, 2015, **44**, 5148.
2 J. D. Benck, T. R. Hellstern, J. Kibsgaard, P. Chakthranont, T. F. Jaramillo, *ACS Catal.,* 2014, **4**, 3957.
3 Zeng, M.; Li, Y. *J. Mater. Chem. A,* 2015, **3**, 14942.
4 M. Chhowalla, H. S. Shin, G. Eda, L.-J Li, K. P. Loh, H. Zhang, *Nature Chem.*, 2013, **5**, 263.
5 B. Hinnemann, P. G. Moses, J. Bonde, K. P. Jørgensen, J. H. Nielsen, S. Horch, I. Chorkendorff, J. K. Nørskov, *J. Am. Chem. Soc.*, 2005, **127**, 5308.
6 D. Voiry, H. Yamaguchi, J. Li, R. Silva, D. C. B. Alves, T. Fujita, M. Chen, T. Asefa, V. B. Shenoy, G. Eda, M. Chhowalla, *Nature Mater.*, 2013, **12**, 850.
7 J. Yang, H. S. Shin, *J. Mater. Chem. A*, 2014, **2**, 5979.
8 a) P. C. K. Vesborg, B. Seger, I. Chorkendorf, *J. Phys. Chem. Lett.*, 2015, **6**, 951. b) Z. He, W. Que, *Appl. Mater. Today* 2016, **3**, 23.
9 J. D. Benck, Z. Chen, L. Y. Kuritzky, A. J. Forman, T. F. Jaramillo, *ACS Catal.*, 2012, **2**, 1916.
10 D. Merki, S. Fierro, H. Vrubela, X. Hu, *Chem. Sci.*, 2011, **2**, 1262.
11 H. Vrubel, D. Merkia, X. Hu, *Energy Environ. Sci.*, 2012, **5**, 6136.
12 H. Vrubel, T. Moehl, M. Grätzel, X. Hu, *Chem. Commun.*, 2013, **49**, 8985.
13 X. Ge, L. Chen, L. Zhang, Y. Wen, A. Hirata, M. Chen, *Adv. Mater.*, 2014, **26**, 3100.
14 S. M. Tan, M. Pumera, *ACS Appl. Mater. Interfaces*, 2016, **8**, 3948.
15 S. Chen, J. Duan, Y. Tang, B. Jin, S. Z. Qiao, *Nano Energy*, 2015, **11**, 11.
16 S. Murugesan, A. Akkineni, B. P. Chou, M. S. Glaz, D. A. V. Bout, K. J. Stevenson, *ACS Nano*, 2013, **7**, 8199.
17 Z. Huang, C. Wang, Z. Chen, H. Meng, C. Lv, Z. Chen, R. Han, C. Zhang, *ACS Appl. Mater. Interfaces*, 2014, **6**, 10408.
18 a) A. Sobczynski, A. Yildiz, A. J. Bard, A. Campion, M. A. Fox, T. Mallouk, S. E. Webber, J. M. White, *J. Phys. Chem.*, 1988, **92**, 2311. b) S. Li, S. Wang, D.-M. Tang, W. Zhao, H. Xu, L. Chu, Y. Bando, D. Golberg, G. Eda, *Appl. Mater. Today* 2015, **1**, 60.
19 J. Gao, B. Li, J. Tan, P. Chow, T.-M. Lu, N. Koratkar, *ACS Nano*, 2016, **10**, 2628.
20 Y.-C. Lin, W. Zhang, J.-K. Huang, K.-K. Liu, Y.-H. Lee, C.-T. Liang, C.-W. Chu, L.-J. Li, *Nanoscale*, 2012, **4**, 6637.
21 A. Ennaoui, S. Fiechter, K. Ellmer, R. Scheer, K. Diesner, *Thin Solid Films*, 1995, **261**, 124.
22 H. Liu, N. Han, J. Zhao, *RSC Adv.*, 2015, **5**, 17572.
23 A. Y. S. Eng, A. Ambrosi, Z. Sofer, P. Simek, M. Pumera, *ACS Nano*, 2014, **8**, 12185.
24 A. Ambrosi, Z. Sofer, M. Pumera, *Small*, 2015, **11**, 605.
25 G. Eda, H. Yamaguchi, D. Voiry, T. Fujita, M. Chen, M. Chhowalla, *Nano Lett.*, 2011, **11**, 5111.

26 L. Wang, Z. Sofer, J. Luxa, M. Pumera, *Adv. Mater. Interfaces*, 2014, **2**, doi: 10.1002/admi.201500041.
27 T. Weber, J. C. Muijsers, J. W. Niemantsverdriet, *J. Phys. Chem.*, 1995, **99**, 9194.
28 J. Kibsgaard, T. F. Jaramillo, F. Besenbacher, *Nature Chem.*, 2014, **6**, 248.
29 Y. Li, Y. Yu, Y. Huang, R. A. Nielsen, W. A. Goddard, Y. Li, L. Cao, *ACS Catal.*, 2015, **5**, 448.
30 J. Duan, S. Chen, M. Jaroniec, S. Z. Qiao, *ACS Catal.*, 2015, **5**, 5207.
31 Y. H. Li, P. F. Liu, L. F. Pan, H. F. Wang, Z. Z. Yang, L. R. Zheng, P. Hu, H. J. Zhao, L. Gu, H. G. Yang, *Nat. Commun.*, 2015, **6**, 8064.
32 S.-J. Choi, S. Chattopadhyay, J. J. Kim, S.-J. Kim, H. L. Tuller, G. C. Rutledge, I.-D. Kim, *Nanoscale*, 2016, **8**, 9159.
33 Y. Pihosh, I. Turkevych, K. Mawatari, J. Uemura, Y. Kazoe, S. Kosar, K. Makita, T. Sugaya, T. Matsui, D. Fujita, M. Tosa, M. Kondo, T. Kitamori, *Sci. Rep.*, 2015, **5**, 11141.
34 L. Yang, X. Zhu, S. Xiong, X. Wu, Y. Shan, P. K. Chu, *ACS Appl. Mater. Interfaces*, 2016, **8**, 13966.
35 J. Song, Z.-F. Huang, L. Pan, J.-J. Zou, X. Zhang, L. Wang, *ACS Catal.*, 2015, **5**, 6594.
36 P. D. Tran, T. V. Tran, M. Orio, S. Torelli, Q. D. Truong, K. Nayuki, Y. Sasaki, S. Y. Chiam, R. Yi, I. Honma, J. Barber, V. Artero, *Nature Mater.*, 2016, **15**, 640.
37 J. Xie, J. Zhang, S. Li, F. Grote, X. Zhang, H. Zhang, R. Wang, Y. Lei, B. Pan, Y. Xie, *J. Am. Chem. Soc.*, 2013, **135**, 17881.
38 H. Li, C. Tsai, A. L. Koh, L. Cai, A. W. Contryman, A. H. Fragapane, J. Zhao, H. S. Han, H. C. Manoharan, F. Abild-Pedersen, J. K. Nørskov, X. Zheng, *Nature Mater.*, 2015, **15**, 48.
39 H. Wang, Z. Lu, S. Xu, D. Kong, J. J. Cha, G. Zheng, P.-C. Hsu, K. Yan, D. Bradshaw, F. B. Prinz, Y. Cui, *Proc. Natl. Acad. Sci. U. S. A.*, 2013, **110**, 19701.
40 Y. Yan, B. Xia, N. Li, Z. Xu, A. Fisher, X. Wang, *J. Mater. Chem. A*, 2015, **3**, 131.
41 D. Wang, Z. Pan, Z. Wu, Z. Wang, Z. Liu, *J. Power Sources*, 2014, **264**, 229.
42 C. L. Choi, J. Feng, Y. G. Li, J. Wu; A. Zak, R. Tenne, H. J. Dai, *Nano Res.*, 2013, **6**, 921.
43 Y. Li, H. Wang, L. Xie, Y. Liang, G. Hong, H. Dai, *J. Am. Chem. Soc.*, 2011, **133**, 7296.
44 J. Kibsgaard, Z. Chen, B. N. Reinecke, T. F. Jaramillo, *Nature Mater.*, 2012, **11**, 963.